Full Characterization of Packaged Er–Yb-Codoped Phosphate Glass Waveguides

Juan A. Vallés, Miguel A. Rebolledo, and Jesús Cortés

***Abstract*—We present a procedure for the characterization of packaged Er–Yb-codoped phosphate glass waveguides. The procedure is based on precise measurements of the output optical powers when the waveguide is diode-laser pumped at 980 nm. The dependence of these optical powers on the input pump power is then fitted to the results from a numerical model that describes in detail the propagation of the optical powers inside the waveguide. The best fit is obtained for the following parameters: the signal wavelength scattering losses are $\alpha(1534) = 8.3 \times 10^{-2}$ dB/cm, the Yb^{3+} absorption and emission cross sections (≈980 nm) are 5.4×10^{-25} m^2 and 7.0×10^{-25} m^2, the Er^{3+} absorption and emission cross sections (≈980 nm) are 1.6×10^{-25} m^2 and 1.2×10^{-25} m^2, the Yb^{3+}–Er^{3+} energy-transfer coefficient is 1.8×10^{-23} m^3/s and the cooperative-upconversion coefficient is 8×10^{-25} m^3/s. An approximate method is introduced that allows the determination of the absorption and emission cross section distributions for the erbium $^4I_{13/2} \Leftrightarrow {}^4I_{15/2}$ transition from the amplified spontaneous emission power spectrum.**

***Index Terms*—Characterization, Er–Yb codoping, integrated optics, optical waveguides.**

I. Introduction

ERBIUM-DOPED waveguides are recently presenting a great technological interest because of their use as amplifiers in high functionality integrated structures and as cw or pulsed tunable laser sources for optical communications, optical storage, medical applications, etc. [1]. The optimization of the performance of these devices require, on the one hand, a continuous improvement in integrated waveguides fabrication techniques and, on the other, an important effort in what regards characterization and modeling.

Usually, the characterization measurements of rare-earth doped materials have been performed on homogeneously-doped bulk samples with a known concentration using solid state lasers or flash-lamp pump [2], [3]. Since waveguide fabrication processes (in-diffusion, ion exchange,...) may introduce changes in the characteristic parameters of the material, rare-earth doped waveguide characterization should preferably be made on the waveguide (*in situ* techniques) to get more precise results. In the case of transversally accessible waveguides, new *in situ* characterization techniques using laser-diode pump have been recently developed, that allow the determination of the absorption and emission cross section distributions for several transitions of the erbium ion [4], [5], even when they are polarization-dependent [6], and of some other parameters as cooperative upconversion coefficients or excited states absorption cross sections [7]. However, since for any practical application a stable performance of the device is mandatory, a pigtailed input and output light coupling has to be used and the waveguide module has to be packaged for isolation and protection. This impedes any transversal access to the waveguide and forces to develop new characterization techniques, exclusively based on in- and outcoupled optical powers, if for instance, the waveguide module is going to be used as the active medium for a laser system whose design is to be modeled and optimized.

In this paper, we present a characterization procedure that allows to determine most of the waveguide relevant parameters. In Section II, the Er^{3+}–Yb^{3+}-codoped system in phosphate glass is analyzed in detail and the characteristic parameters that have to be determined are studied. Phosphate glass are excellent for rare-earth host materials and the ytterbium codoping offers the advantage of a ytterbium large absorption cross section near 980 nm and a good spectral overlap of its emission with the erbium $^4I_{11/2}$ absorption, leading to an efficient energy transfer from ytterbium to erbium [8]. In Section III, the experimental aspects are considered, the setup that was built using the waveguide that was going to be characterized and the measurements of pump power attenuation, copropagating amplified spontaneous emission (ASE^+) power and signal gain are described. In Section IV the numerical model for the propagation of the optical powers and the experimental/numerical fitting process are detailed. In Section V, the resulting best-fit parameters are summarized and discussed, and the comparison between experimental and numerical results is shown. In Section VI, the absorption and emission cross sections distributions for the erbium ion $^4I_{13/2} \Leftrightarrow {}^4I_{15/2}$ transition are also determined from the experimental ASE^+ power spectrum by assuming as an approximation their uncoupled evolution along the waveguide. Finally, the conclusions are summarized in Section VII.

II. Er^{3+}–Yb^{3+}-Codoped System in a Phosphate Glass Waveguide

A. Er^{3+}–Yb^{3+}-Codoped System

Phosphate glasses are known to be excellent for rare-earth host materials in terms of their spectroscopic characteristics, and have been widely used for bulk laser applications. For waveguiding configurations the high Er^{3+}-doping concentra-

Manuscript received June 6, 2005; revised September 14, 2005. This work was supported by the Comisión Interministerial de Ciencia y Tecnología, project TIC2003-03192 of the Programa Nacional de Tecnología de la Información y Telecomunicaciones.

J. A. Vallés and M. A. Rebolledo are with the Department of Applied Physics, Faculty of Sciences, 50009 Zaragoza, Spain and also with the Aragón Institute for Engineering Research (I3A), Zaragosa 50018, Spain (e-mail: juanval@unizar.es).

J. Cortés is with the Department of Applied Physics, Faculty of Sciences, 50009 Zaragoza, Spain (e-mail: marebo@unizar.es; 492506@unizar.es).

Digital Object Identifier 10.1109/JQE.2005.861825

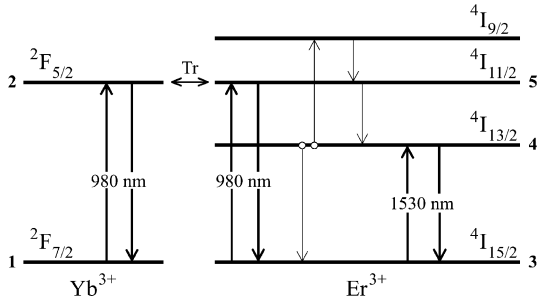

Fig. 1. Energy level scheme of the Yb^{3+} – Er^{3+}-codoped system in a phosphate glass.

tions ($> 10^{26}$ ions/m^3) that are required in order to achieve the high gain within a few centimeters of length (that the integrated optics active components need) can be doped into phosphate glass without serious ion clustering because of their high solubility for rare earth ions [3]. However, the pumping efficiency of the active devices is seriously limited because of the relatively low absorption cross section of the Er^{3+} ions for the usual pumping wavelengths. This pumping efficiency can be enlarged by using Yb^{3+} as codopant. In Fig. 1 the schematic energy-level diagram of an Er^{3+}–Yb^{3+}-codoped system in phosphate glasses for amplification in 1.5 μm and considering a 980-nm pump wavelength is shown.

1) Er^{3+} Energy Levels: As can be seen in Fig. 1 the energy levels of the 980-nm pumped Er^{3+} ion for optical amplification at 1.5 μm form a three-level system, which requires a high pump rate to achieve population inversion. The laser transition takes place between the $^4I_{13/2}$ level and the ground level, $^4I_{15/2}$. The spontaneous decay from level $^4I_{13/2}$ to $^4I_{15/2}$ is essentially radiative. Spontaneous decays form levels $^4I_{11/2}$ and $^4I_{9/2}$, instead, are predominantly nonradiative, since energy gaps between levels $^4I_{13/2}$ and $^4I_{11/2}$, and levels $^4I_{11/2}$ and $^4I_{9/2}$ are small compared to the maximum phonon energy of the phosphate glass matrix. Since the decay from level $^4I_{9/2}$ ($A_6 = 3.5 \times 10^8$ s^{-1}) [9] is fast compared with pump rate, the population of this level is from now on assumed to be negligible. Higher erbium levels are not involved in the population dynamics because the effect of excited state absorption is negligible with pumping in the 940–980-nm region [10] in contrast to pumping at around 800 nm.

2) Cooperative Upconversion Process: As can be seen in Fig. 1, the main loss channel that limits gain performance in the high Er^{3+}-doped phosphate glasses is the cooperative-upconversion process. In general, several energy transfer processes are involved in high Er concentration materials [11]. For amplifier applications using oxide glasses, such as silica, silicate and phosphate, the cooperative upconversion processes associated with the energy transfer between Er^{3+} ions excited at $^4I_{13/2}$ level is the most significant [12]. Due to the weak interaction among the rare earth ions, phosphate glasses present a small cooperative upconversion rate (one order of magnitude smaller than in silica glass [9]) and also its increase with the increase of Er^{3+} was found to be small, allowing Er^{3+} concentrations even higher than 3.7×10^{26} m^{-3} [9].

3) Yb–Er Energy Transfer: The Yb^{3+} ion has only two levels, the ground state $^2F_{7/2}$ and the excited level $^2F_{5/2}$, whose spontaneous decay is essentially radiative. Compared to the erbium ones, ytterbium ions exhibit a large absorption cross section near 980 nm [13] and, therefore, pump radiation is mostly absorbed by these ions. However, the large spectral overlap between Yb^{3+} emission ($^2F_{5/2} \Rightarrow {}^2F_{7/2}$) and Er^{3+} absorption ($^4I_{15/2} \Rightarrow {}^4I_{13/2}$) results in an efficient resonant energy transfer from Yb^{3+} to Er^{3+} in the Er^{3+}–Yb^{3+}-codoped system. Although the back-transfer mechanism from erbium to ytterbium is also possible, the large phonon energy in the phosphate host increases the transition probability for the $^4I_{11/2} \Rightarrow {}^4I_{13/2}$ relaxation, which prevents a significant back energy-transfer from Er^{3+} to Yb^{3+} [14]. This fact makes phosphate glass, when compared with other materials, an ideal host for an Er^{3+}–Yb^{3+}-codoped system.

4) Rate Equations: Therefore, the rate equations for this system, which describe the temporal evolution of the population densities of the levels n_i can be written

$$\frac{dn_2}{dt} = W_{12}n_1 + C_{52}n_5n_1 - [A_2 + W_{21}]n_2 - C_{25}n_2n_3 \quad (1)$$

$$\frac{dn_4}{dt} = W_{34}n_3 - [A_4 + W_{43}]n_4 - 2C_{44}n_4^2 + A_5n_5 \quad (2)$$

$$\frac{dn_5}{dt} = C_{25}n_2n_3 + W_{35}n_3 - C_{52}n_1n_5 - [A_5 + W_{53}]n_5 + C_{44}n_4^2 \quad (3)$$

$$n_1 + n_2 = n_{Yb} \quad (4)$$

$$n_3 + n_4 + n_5 = n_{Er} \quad (5)$$

where the population densities of the ytterbium levels $^2F_{7/2}$ and $^2F_{5/2}$, and of the erbium levels $^4I_{15/2}$, $^4I_{13/2}$, and $^4I_{11/2}$ are represented by $n_1(x,y,z)$, $n_2(x,y,z)$, $n_3(x,y,z)$, $n_4(x,y,z)$, and $n_5(x,y,z)$ respectively. Moreover, the z-independent ytterbium and erbium concentration profiles are denoted as n_{Yb} and n_{Er}. In (1)–(5), A_i represent the spontaneous relaxation rates, whereas C_{44} is the homogeneous upconversion coefficient and C_{25} and C_{52} are, respectively, the energy transfer and back transfer coefficients.

The values of the densities of stimulated radiative transition rates $W_{ij}(x,y,z)$ can be obtained using

$$W_{ij}(x,y,z) = \sum_{\nu} \frac{\sigma_{ij}(\nu)}{h\nu} \Psi(x,y,\nu) \times P(z,\nu) \quad (6)$$

where $\Psi(x,y,z)$ is the normalized intensity modal distribution of the pump, signal or ASE waves, which depends on the waveguide geometry and index profile and is assumed to be z-independent and $P(z,\nu)$ are the total optical powers. Finally, $\sigma_{ij}(\nu)$ are the cross sections corresponding to the transition between the ith and jth levels. Notice that in (1)–(5), the spatial dependence of the population densities and those of the densities of stimulated radiative transition rates are omitted for simplicity.

B. Characterization Techniques for Packaged Waveguides

Most of the parameters of the Er^{3+}–Yb^{3+}-codoped system that are available in the literature have been obtained from measurements on bulk samples by using rate equations analysis [8],

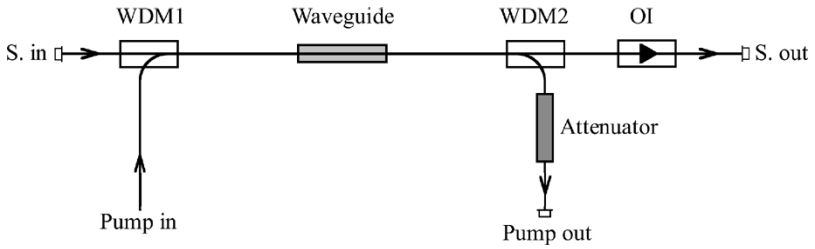

Fig. 2. Experimental setup scheme.

[9], [11]. However, for packaged waveguides the unavoidable longitudinal measurements not only involve the population dynamics but also the propagation of the optical powers along the active waveguide, what enormously complicates the analysis of the experimental results. As can be easily understood, this analysis requires both very precise measurements and a detailed and reliable optical powers propagation model, which are described in the next sections.

III. Experimental

For the experiments a 5.5-cm-long channel waveguide was used. The waveguide section was 6×4 μm^2, the distance from the waveguide axis to the glass surface is 7 μm and the refractive index change at the peak of the index profile is approximately 0.04. The buried waveguide was fabricated by Teem Photonics using a two-step ion exchange process in a phosphate glass codoped with Er–Yb ions (Er^{3+} and Yb^{3+} concentrations are 2.0×10^{26} ions/m^3 and 2.2×10^{26} ions/m^3, respectively). The waveguide is pigtailed at both ends in order to allow an efficient input/output coupling of the optical powers.

A. Experimental Setup

Our characterization technique is based on the measurement of the pump power attenuation, the output ASE^+ powers and the small signal gain of the waveguide. Fig. 2 shows the experimental setup. A 980-nm semiconductor pump laser diode was used and an optical isolator at the pump laser output end avoided any significant backward reflection that may have unstabilized the laser diode. Two 980/1550-nm wavelength division multiplexers (WDMs) allow the incoupling of pump and copropagating signal and the outcoupling of the amplified signal, the remaining pump and the ASE^+. The outcoupled pump power was further attenuated in order to match the linear behavior range of the power meter. Finally, in order to avoid auto-oscillation phenomena, an optical isolator was coupled at the copropagating output of the waveguide amplifier.

All the components in the setup were carefully calibrated (WDMs, connectors, pump power attenuator, and optical isolator). These calibrations are required to accurately estimate the optical powers at the waveguide ends from the measured optical powers. Passive losses of the waveguide (scattering and insertion losses) could not be directly measured and were estimated to be slightly lower than 1 dB in the 1.3-μm band. The output power of the pump laser was also calibrated.

B. Measurements

1) Measurements of the Pump Power Attenuation and ASE^+ Power Spectrum: Measurements were carried out for a large pump power range. The lowest pump power value (for a 100-mA drive current) was chosen to be the one that guaranteed that the spontaneous emission power near 980 nm was less than 1% of the laser power. The maximum available pump power at the waveguide input end was measured to be 356 mW (for a 900-mA drive current). The outcoupled pump power went through the attenuator and was measured by a power meter for nine equally spaced values of the laser-diode drive-current intensity. From the values of the in- and output pump powers and the calibration of the passive losses of the components, pump power attenuation of the waveguide was obtained. For the same drive current intensities we registered the ASE^+ power spectra from 1480 to 1620 nm with an optical spectrum analyzer (OSA). The spectral resolution was 1 nm. By subtracting the OSA background noise profile and taking into account all the above-mentioned calibrations, we determined the ASE^+ spectra at the waveguide output end.

2) Measurements of Small Signal Gain: A tunable laser was used as signal source with an approximate output power of 5 μW. We checked that the presence of this small signal power had no influence in the ASE^+ powers. First, the copropagating spectral gain of the amplifier was measured for a pump-diode drive current of 900 mA and the gain spectrum of the waveguide was obtained from it. The gain spectrum width was some tenths of nanometer and the gain peak value was 19.2 dB for a signal wavelength of 1534 nm. Finally, we measured for this wavelength, 1534 nm, the signal gain of the waveguide as a function of the input pump power.

IV. Propagation Model and Fitting Method

The comparison of the experimental results of the waveguide performance with any numerical ones, in order to determine the waveguide parameters, requires the use of a reliable numerical model. We have adapted to the Er^{3+}–Yb^{3+}-codoped system in phosphate glass the model presented in [15] for Er-doped Ti:$LiNbO_3$ waveguides. This model describes the propagation of the optical powers along the active waveguide as a function of its characteristic parameters. In [15], this model was successfully tested by comparing gain and ASE measurements and numerical results, after the experimental determination of most of the waveguide parameters.

A. Propagation of the Optical Powers

The evolution along the active waveguide of the pump, signal and ASE powers can be expressed as follows:

$$\frac{dP_p(z,\nu_p)}{dz} = \sigma_{53}(\nu_p)N_5(z,\nu_p) - \sigma_{35}(\nu_p)N_3(z,\nu_p) + \sigma_{21}(\nu_p)N_2(z,\nu_p) - \sigma_{12}(\nu_p)N_1(z,\nu_p) - \alpha(\nu_p) \quad (7)$$

$$\frac{dP_s(z,\nu_s)}{dz} = \sigma_{43}(\nu_s)N_4(z,\nu_s) - \sigma_{34}(\nu_s)N_3(z,\nu_s) - \alpha(\nu_s) \quad (8)$$

$$\frac{dP_f^{\pm}(z,\nu_f)}{dz} = \pm 2h\nu_f\Delta\nu_f\sigma_{43}(\nu_f) \pm [\sigma_{43}(\nu_f)N_4(z,\nu_f) - \sigma_{34}(\nu_f)N_3(z,\nu_f) - \alpha(\nu_f)]P_f^{\pm}(z,\nu_f). \quad (9)$$

In (7)–(9) $P_\gamma^{\pm}(z,\nu_\gamma)$ are the optical powers, where z is the distance along the waveguide axis and the label γ is p for pumping, s for signal, and f for ASE. The pump and the signal are assumed to be monochromatic whereas the ASE is polychromatic because of the polychromaticity of the spontaneous emission. The ASE spectrum can be divided into small slots of width $\Delta\nu_f$, so that $P_f^{\pm}(z,\nu_f)$ represents the power in a slot around frequency ν_f, and the superscript "+" denotes copropagating waves whereas "-" indicates counterpropagating waves along the z axis. The wavelength-dependent scattering losses are denoted as $\alpha(\nu_\gamma)$ and their λ dependence is assumed to follow the Rayleigh λ^{-4} law. Finally, in (7)–(9) the coupling parameters, $N_i(z,\nu_s)$, are the overlapping integrals between the ith level population density distribution and the normalized intensity modal distribution over A, the active area

$$N_i(z,\nu) = \iint_A \Psi(x,y,\nu)n_i(x,y,z)dxdy. \quad (10)$$

As in [15], and due to the fact that not only the waveguide region is Er–Yb-codoped, the active area is defined as the one for which the integral of the sum of population densities of the excited levels converges within a required precision.

The equations that describe the propagation of the optical powers along the waveguide, (7)–(9), are numerically integrated through a Runge-Kutta-based iterative procedure. Co- and counterpropagating amplified spontaneous emission, $\text{ASE}^{\pm}$, are spectrally resolved into 140 frequency slots between 1480 and 1620 nm.

B. Initial Values

As initial values of the characteristic parameters for our computation we have used some realistic values either provided by the waveguide supplier or taken form the literature. We also made a few reasonable assumptions:

1) Spontaneous Radiative and Nonradiative Relaxation Rates: We have assumed the values given by the waveguide supplier, $A_2 = 1/(1.1 \times 10^{-3})\ \text{s}^{-1}$ and $A_4 = 1/(7.3 \times 10^{-3})\ \text{s}^{-1}$, since they fully agree with the ones in [16], [17]. For A_5 we assumed the one in [9], $A_5 = 3.6 \times 10^5\ \text{s}^{-1}$.

2) Absorption and Emission Cross Sections: We assume that McCumber theory is fully applicable for this system [18]. Therefore, emission cross sections $\sigma_{\text{e}}(\nu)$ can be obtained from the absorption cross sections $\sigma_{\text{a}}(\nu)$ by using McCumber relation

$$\sigma_e(\nu) = \sigma_a(\nu)\exp\left(\frac{\varepsilon_T - h\nu}{kT}\right) \quad (11)$$

which was demonstrated to be applicable to rare earth ions and to provide more accurate cross sections values than the Ladenburg–Fuchtbauer analysis [19]. In (11), ε_T is a temperature-dependent effective excitation energy. As initial values for the Yb and Er absorption cross sections we took $\sigma_{12}(980) = 5.2 \times 10^{-25}\ \text{m}^2$ and $\sigma_{35}(980) = 1.6 \times 10^{-25}\ \text{m}^2$ [13]. The rates between absorption and emission cross sections for 980-nm pump wavelength for the ions Yb^{3+} and Er^{3+}, that we keep along the fitting process, were found to be $\sigma_{21}/\sigma_{12} \simeq 1.3$ [13] and $\sigma_{53}/\sigma_{35} \simeq .78$ [4]. In what regards the absorption cross section distribution for the ${}^4I_{13/2} \Leftrightarrow {}^4I_{15/2}$ transition, we assumed as an initial relative distribution profile the one in [20], corrected with the value $\sigma_{34}(1535) = 6.6 \times 10^{-25}\ \text{m}^2$ (given by the waveguide supplier), and have obtained the emission cross section values by using McCumber equation with $\varepsilon_T = 6512.0\ \text{cm}^{-1}$ [4]. This value was obtained for a Ti:Er:$LiNbO_3$ waveguide and may change for the Yb–Er-codoped system in a phosphate glass.

3) Mode Intensity: The mode intensity profiles are assumed to be Gaussian and to have 5 and 6 μm diameters for 980 and 1534 nm, respectively. These data were also provided by the waveguide supplier.

4) Losses: The waveguide supplier indicated that propagation losses were lower than 0.1 dB/cm at 1.5 μm. Insertion losses are evaluated from the waveguide and pigtail-fiber mode intensity profile diameters (3.94 and 5.86 μm diameters for 980 and 1534 nm, respectively) to be negligible for the signal wavelength and 0.12 dB for 980 nm.

5) Other Parameters: The cooperative upconversion coefficient was taken from [11] for similar Yb and Er concentrations, $C_{44} = 7 \times 10^{-25}\ \text{m}^3/\text{s}$. Energy transfer ($C_{25} = 1.5 \times 10^{-23}\ \text{m}^3/\text{s}$) and back-transfer coefficients ($C_{52} = 1.5 \times 10^{-22}\ \text{m}^3/\text{s}$) were taken from the waveguide supplier and from [17], respectively.

For simplicity, the same mode intensity profile and scattering losses than for the signal wavelength can be assumed for all the wavelengths in the 1.5-μm ASE band, without any noticeable effect in the results.

C. Fitting Method

From (7)–(9), it can be appreciated that some unknown parameters have a more direct influence on the pump power evolution, while some others have a more direct influence on the signal or ASE evolution, and only an indirect one on the pump power's. Due to this fact, we can separate the set of parameters to be determined into two subsets and carry out two different fitting processes.

1) Fitting of the Pump Power Attenuation Measurements: We compute the attenuation of the pump power inside the waveguide as a function of the input pump power and fit this dependence to the experimental results. The three fitting parameters used in this process are the signal-wavelength scattering losses, $\alpha(1534)$, and the ytterbium and erbium absorption cross sections at the pump wavelength, $\sigma_{12}(980)$ and $\sigma_{35}(980)$. Whereas

the influence on the pump power attenuation of the changes in the scattering losses values is in practice independent of the input pump power, the rate between the absorbing terms in (7) $(\sigma_{12}(\nu_p)N_1(z,\nu_p)/\sigma_{35}(\nu_p)N_3(z,\nu_p))$ strongly depends on the input pump power, mostly because of differences in evolution of the overlapping integral caused by the different level structure.

2) Fitting of the Small Signal Gain and ASE$^+$ Total Power: We compute the small signal gain and the total ASE$^+$ power as a function of the input pump power. The signal wavelength is 1534 nm, the peak wavelength in the spectral gain measurements. The four fitting parameters are now the erbium absorption cross sections at the signal wavelength, $\sigma_{34}(1534)$, the upconversion and energy transfer coefficients, C_{44} and C_{25}, and the effective excitation energy ε_T. Since the influence of the effective excitation energy is a small one, in practice, the dependence of the small signal gain for the peak wavelength on the input pump power can be fitted using the other three free parameters, and then the effective excitation energy value is slightly corrected using the ASE$^+$ total power. As it happened with the fitting-process first step, each parameter has a different influence depending on the pump power range. Energy-transfer coefficients have a larger influence at low pump intensities, when the population in the level $^4I_{13/2}$ is small and the cooperative upconversion effect for the Er^{3+} ions is negligible, whereas the cooperative upconversion coefficient has a more significant role at higher pump intensities. We have not included in the fitting parameters set the back transfer coefficient because its influence on signal gain for these dopant concentrations, even for the maximum pump power available, is not significant. We have calculated that for a 900-mA drive current, the population of level $^4I_{11/2}$ is approximately 0.04% of the Er concentration for the highest pump power and the term $C_{52}n_1n_5$ in the rate equations system is always relatively small. Finally, a change in the effective excitation energy ε_T slightly affects the rate between emission and absorption cross sections for a given wavelength, but noticeably influences the total ASE$^+$ power value.

V. Results and Discussion

The best fit is obtained for the values of the parameters that are compiled in Table I. Emission cross sections are obtained from the fitted values of the absorption cross sections by means of the McCumber formula (11). The value for the signal wavelength scattering losses agrees with the value provider by supplier (lower than 0.1 dB/cm) and the associated scattering losses along the whole waveguide length for 1.3 μm are 0.88 dB, which is also in good agreement with our measurements (slightly lower than 1 dB). All the absorption cross sections present a good agreement with values by other authors [13] and so does the cooperative upconversion coefficient [13]. The energy transfer coefficients obtained only differ 20% from the value given by the supplier but are half the values from other works [13]. The small effective excitation energy value change reflects the shift in the peak value when the ASE$^+$ spectrum is compared with the ones form a Ti:Er.$LiNbO_3$ waveguide. The global 2.5-nm shift in the wavelength that verifies that the absorption and emission cross sections coincide, means only a 5% change in the absorption/emission cross section rate for the peak wavelength. The uniqueness of the best-fit parameters is guaranteed by the different influence of each free parameter depending on the input power range. In our fitting process we searched for the lower-error two-digits parameter set. The unavoidable error in optical power measurements does not allow any further accuracy.

In Fig. 3, it is shown the measured pump attenuation and signal gain and the numerical values for the best-fit parameters as a function of the laser diode drive current. The agreement for all the pump power ranges is excellent. Another remarkable aspect is that not only relative measurements have been used for the fitting process but also the absolute values of the total ASE$^+$ power. In Fig. 4 the measured total ASE$^+$ power (as a function of the laser diode drive current) and the numerical values for the best-fit parameters are shown. The experimental/numerical agreement is also excellent.

TABLE I
Experimental/Numerical Best-Fit Parameters

BEST-FIT PARAMETERS	
Scattering losses:	
$\alpha(1534) = 8.3\times10^{-2}\,dB/cm$	
Absorption/emission cross sections:	
$\sigma_{12}(980) = 5.4\times10^{-25}\,m^2$	$\sigma_{21}(980) = 7.0\times10^{-25}\,m^2$
$\sigma_{35}(980) = 1.6\times10^{-25}\,m^2$	$\sigma_{53}(980) = 1.2\times10^{-25}\,m^2$
$\sigma_{34}(1534) = 5.4\times10^{-25}\,m^2$	$\sigma_{43}(1534) = 5.3\times10^{-25}\,m^2$
Upconversion coefficient:	
$C_{44} = 8\times10^{-25}\,m^3/s$	
Energy transfer rate:	
$C_{25} = 1.8\times10^{-23}\,m^3/s$	
Effective excitation energy	
$\varepsilon_T = 6514.7\,cm^{-1}$	

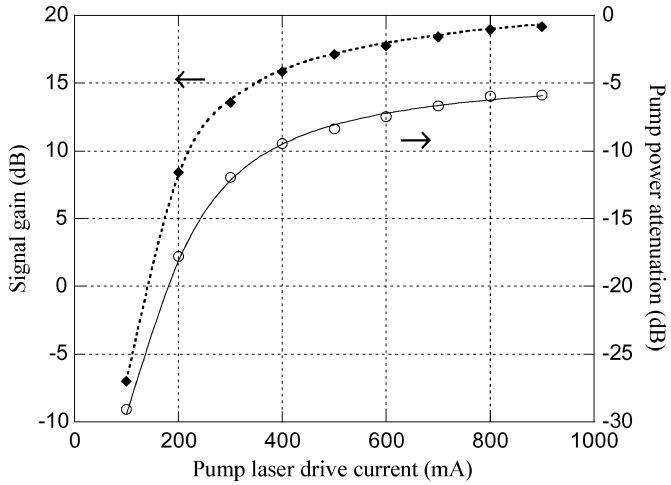

Fig. 3. Measured pump attenuation (○) and signal gain (◆) and numerical values (full and broken lines) for the best-fit parameters, as a function of the laser diode drive current.

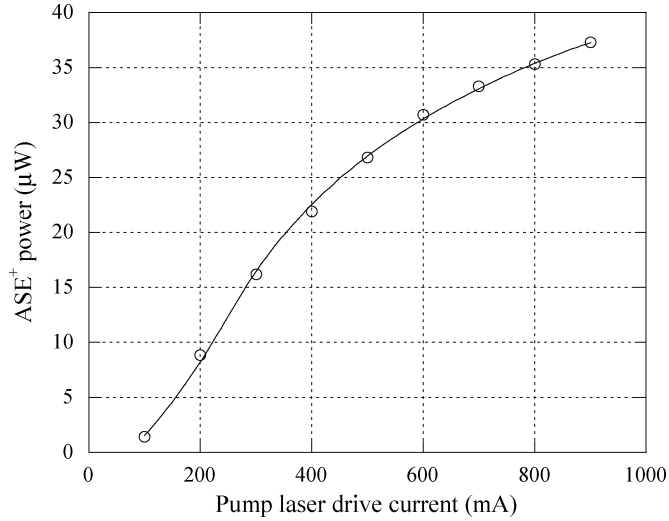

Fig. 4. Measured total ASE^+ power ($\circ$) and numerical (full line) values for the best-fit parameters, as a function of the laser diode drive current.

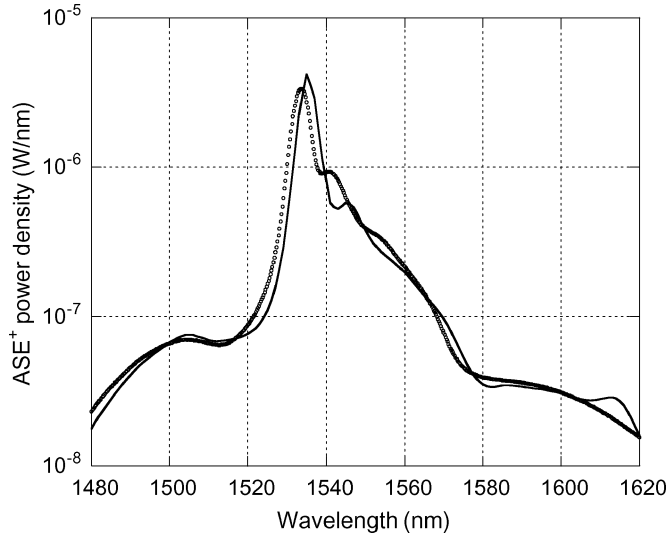

Fig. 5. Measured ($\circ$) and numerical (full line) ASE^+ power spectrum, for a laser diode drive current of 900 mA ($\approx$356 mW of input pump power).

However, as it could have been expected, some discrepancies show up between the measured and the numerical ASE^+ spectra. In Fig. 5 the experimental and numerical ASE^+ power spectra for a laser diode drive current of 900 mA ($\approx$356 mW of input pump power) are shown. These differences can be assigned in his turn, to small discrepancies in the cross sections distributions. This fact makes us consider a procedure for recalculating the absorption/emission cross sections of the signal band using the measured ASE^+ power spectra.

VI. Spectral Characterization

As we have already mentioned, none of the spectral characterization techniques previously developed by us for transversally accessible waveguides is applicable for packaged devices [4]–[7]. Now only have at our disposal the ASE^+ power spectra. However, each spectrum not only reveals the influence of absorption and emission cross sections, but it is also influenced by the involved propagation of the amplified fluorescence powers along the waveguide. We present an approximate method that simplifies the calculation of this propagation by averaging the influence of each population level along the waveguide on the ASE^+ power propagation.

A. Approximate Method

We assume that the copropagating fluorescence powers inside each wavelength slot, $P_f^+(z,\nu)$, evolve in an uncoupled way (they do not influence each other) along the waveguide and, therefore, each of these evolutions can be fully described using expression (9) which can be further simplified if McCumber relation (11), that is rewritten as $\sigma_e(\nu) = k(\nu)\sigma_a(\nu)$, is applied. It is quite clear that the overlapping integrals, $N_i(z,\nu)$, enormously complicate the calculation of the ASE^+ power propagation. However, as we have already mentioned, for the calculations in Section IV, the same mode intensity profile can be considered for all the wavelengths in the 1.55-μm fluorescence band and, moreover, depending on the working conditions (for high pump powers, for example) the population density of each level, n_i, is nearly constant along the whole active waveguide. Therefore, we assume each overlapping integral to be constant along the waveguide, and introduce two new parameters, $\overline{N_3}$ and $\overline{N_4}$, that average the influence of each level's population over the ASE^+ powers along the whole active waveguide.

Then, by integrating (9), the output ASE^+ power can be expressed as

$$P_f^+(z_T,\nu) = \frac{2h\nu\Delta\nu\sigma_{43}(\nu)\overline{N_4}}{\sigma_{43}(\nu)\left[\overline{N_4} - k(\nu)\overline{N_3}\right] - \alpha(\nu)} \times \left\{ e^{\left\{\sigma_{43}(\nu)\left[\overline{N_4} - k(\nu)\overline{N_3}\right] - \alpha(\nu)\right\} z_T} - 1 \right\} \quad (12)$$

where z_T is the waveguide length.

In order to recalculate the emission and absorption cross sections that best fit the measured ASE^+ spectra we follow a two-step iterative method.

1) We compute the values for $\overline{N_3}$ and $\overline{N_4}$ that best fit the numerical output ASE^+ power spectrum (for a laser diode drive current of 900 mA) that is obtained without any approximation in the propagation of the optical powers.
2) Using the values for $\overline{N_3}$ and $\overline{N_4}$, new approximate emission cross sections, $\sigma_{43}(\nu)$, are evaluated that best fit (12) for each channel of the experimental ASE^+ power spectrum. Finally, the evolution of the optical powers along the waveguide is numerically computed again using the new emission cross sections (and the related absorption ones).

The procedure follows until an adequate convergence is reached between two consecutive loops.

B. Results

At the end of the described process the numerical and experimental ASE^+ spectra for a laser diode drive current of 900 mA totally coincide. In Fig. 6, the numerical and experimental spectra are shown for five input pump powers. A very good agreement is observable not only for the laser diode drive current used in the fitting procedure but also for the other four values. Notice that in Fig. 6, the double scaling is used in order to better notice this agreement.

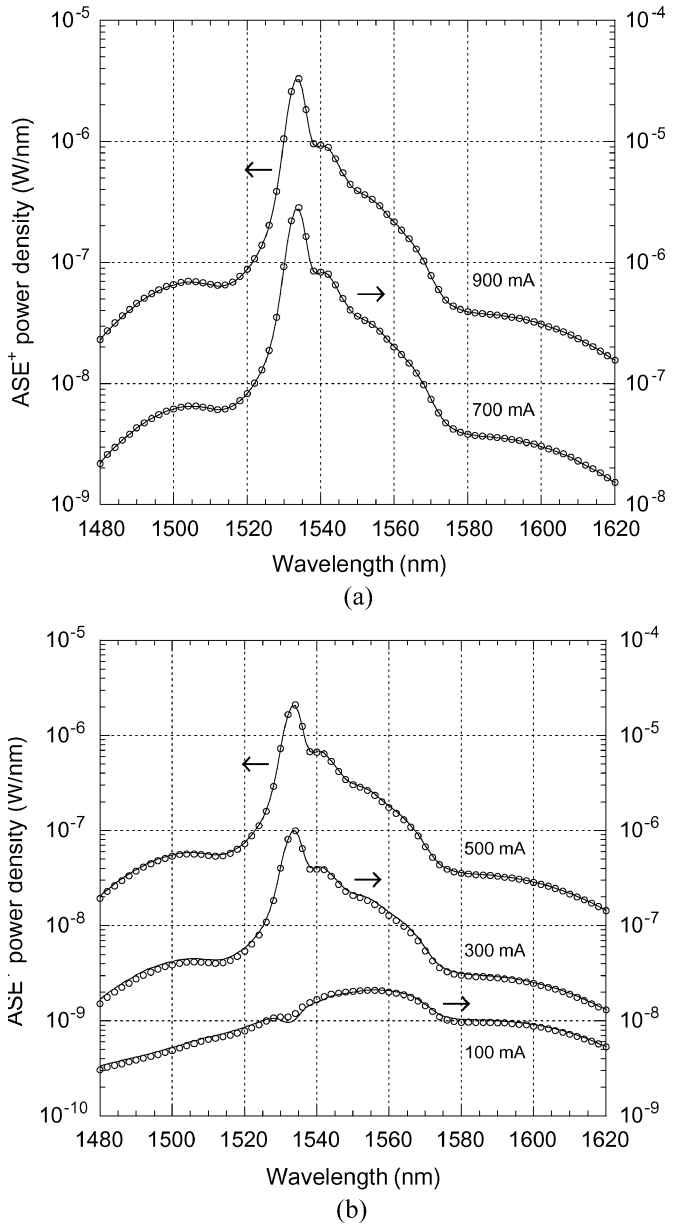

Fig. 6. Measured (∘) and numerical (full line) ASE^{+} power spectra for 5 laser diode drive currents. (a) 900 and 700 mA. (b) 500, 300, and 100 mA.

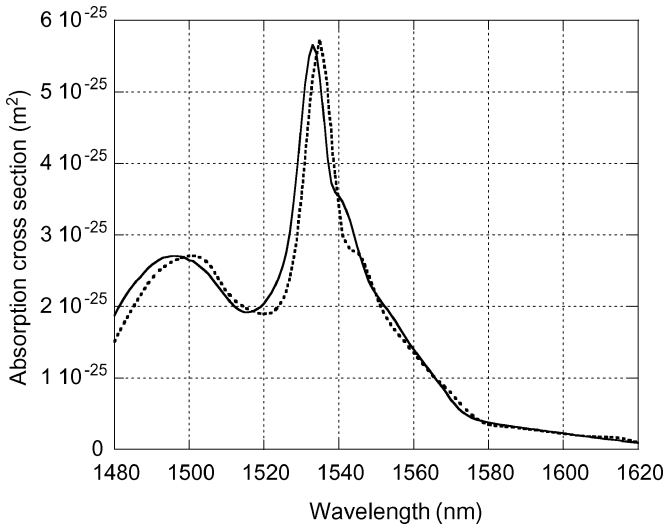

Fig. 7. Initial (broken line) absorption cross section profile (from [18]) and final (full line) profile obtained from the measured ASE^{+} power spectrum for a laser diode drive current of 900 mA.

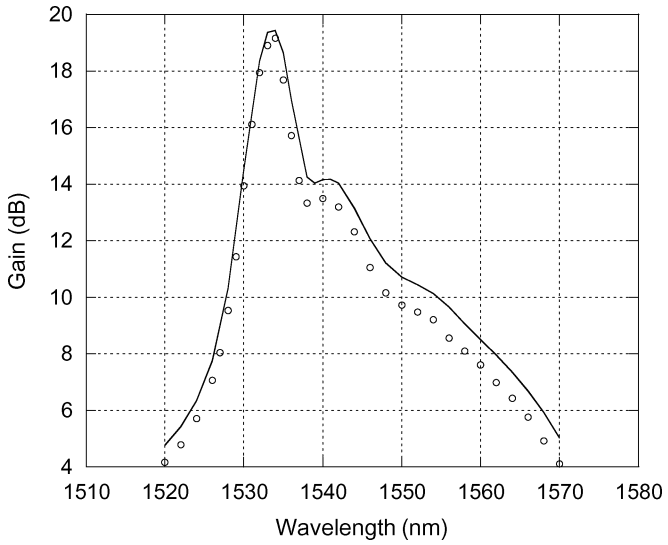

Fig. 8. Measured (∘) and numerical (full line) small signal gain spectrum for a laser diode drive current of 900 mA.

In Fig. 7, the initial absorption cross section profile (from [20]) and the final one (obtained from ASE^{+} measurements) are shown. Finally, in order to further test the new cross section distributions we have calculated the small signal gain spectrum. In Fig. 8, the experimental and numerical spectra are shown. A good agreement can be observed near the peak of the gain profile. However this agreement is not so good for the wavelengths in the band wings. The reason for this disagreement can be attributed to the fact that the finite linewidth of rare-earth transitions generates nonnegligible discrepancies in the spectral wings when McCumber theory is used to obtain cross section values, as it is demonstrated in [21].

The approximated method presented in this section could have been similarly developed by using the small signal gain spectrum measurement and the equation that describes the propagation of the signal power inside the active waveguide (8), instead. Then, a much better agreement would have been obtained for the experimental/numerical gain spectra but a worse one for the ASE^{+} spectra.

VII. Conclusion

In situ characterization techniques for waveguides that are not transversally accessible require both precise measurements of the in- and outcoupled optical powers and a detailed model that incorporates all the mechanisms that influence on the evolution of these optical powers along the active waveguide. When both requirements are fulfilled most of the parameters can be determined, by following a fitting procedure that has into account how relevant is each parameter influence on the propagation of the different optical powers, and the performance of the waveguide for different applications can be accurately predicted. There is a good agreement between the obtained results

and manufacturer's and published data. The desirable comparison with results from transversal spectra was not feasible since the module would surely have been damaged in the necessary unpackaging operation.

REFERENCES

[1] C. Becker, T. Oesselke, J. Pandavenes, R. Ricken, K. Rockhausen, G. Schreiber, W. Sohler, H. Suche, R. Wessel, S. Balsamo, I. Montrosset, and D. Sciancalepore, "Advanced Ti:$LiNbO_3$ waveguide lasers," *IEEE J. Sel. Topics Quantum Electron.*, vol. 6, no. 1, pp. 101–110, Jan//Feb. 2000.

[2] C. Huang, L. McCaughan, and D. M. Gill, "Evaluation of absorption and emission cross sections of Er-doped $LiNbO_3$ for application to integrated optic amplifiers," *J. Lightw. Technol.*, vol. 12, no. 5, pp. 803–809, May 1994.

[3] V. P. Gapontsev, S. M. Matitsin, A. A. Isineev, and V. B. Kravchenco, "Erbium glass lasers and their applications," *Opt. Laser Technol.*, vol. 14, pp. 189–196, 1989.

[4] J. A. Lázaro, J. A. Vallés, and M. A. Rebolledo, "Determination of emission and absorption cross sections of Er^{3+} in $LiNbO_3$ waveguides from transversal fluorescence spectra," *Pure Appt. Opt.*, vol. 7, pp. 1363–1371, 1998.

[5] J. A. Lázaro, J. A. Vallés, and M. A. Rebolledo, "In situ measurement of absorption and emission cross-sections in Er^{3+}-doped waveguides for transitions involving thermalized states," *IEEE J. Quantum Electron.*, vol. 35, no. 5, pp. 827–831, May 1999.

[6] M. A. Rebolledo, J. A. Vallés, and S. Setién, "In situ measurement of polarization-resolved emission and absorption cross-sections of Er-doped Ti:$LiNbO_3$ waveguides," *J. Opt. Soc. Amer. B: Opt. Phys.*, vol. 19, pp. 1516–1520, 2002.

[7] J. A. Vallés, J. A. Lázaro, and M. A. Rebolledo, "Analysis of competing mechanisms in transitions between excited states in Er-doped integrated waveguides," *IEEE J. Quantum Electron.*, vol. 38, no. 3, pp. 318–323, Mar. 2002.

[8] J. F. Philipps, T. Töpfer, H. Ebendorff-Heidepriem, D. Ehrt, and R. Sauerbrey, "Energy transfer and upconversion in erbium-ytterbium-doped fluoride phosphate glasses," *Appl. Phys. B*, vol. 74, pp. 233–236, 2002.

[9] S. Honkanen, T. Ohtsuki, S. Jiang, S. I. Najafi, and N. Peyghambarian, "High Er concentration phosphate glasses for planar waveguide amplifiers," *Proc. SPIE*, vol. 2996, pp. 32–40, 1997.

[10] S. Taccheo, G. Sorbello, S. Longhi, and P. Laporta, "Measurement of the energy transfer and upconversion constants in Er-Yb-doped phosphate glass," *Opt. Quantum Electron.*, vol. 31, pp. 249–262, 1999.

[11] W. Q. Shi, M. Bass, and M. Birnhaum, "Effects of energy transfer among Er^{3+} ions on the fluorescence decay and lasing properties of heavily doped Er:$Y_3Al_5O_{12}$," *J. Opt. Soc. Amer. B*, vol. 7, pp. 1456–1462, 1990.

[12] P. Blixt, J. Nilsson, T. Carlnas, and B. Jaskorzynska, "Concentration-dependent upconversion in Er^{3+}-doped fiber amplifiers: experiments and modeling," *IEEE Photon. Technol. Lett.*, vol. 3, no. 11, pp. 996–998, Nov. 1991.

[13] B.-C. Hwang, S. Jiang, T. Luo, J. Watson, G. Sorbello, and N. Peyghambarian, "Cooperative upconversion and energy transfer of new high Er^{3+} and $Yb^{3+} - Er^{3+}$-doped phosphate glasses," *J. Opt. Soc. Amer. B*, vol. 17, no. 5, pp. 833–839, May 2000.

[14] E. F. Artemev, A. G. Murzin, Y. K. Federov, and V. A. Fromzel, "Some characteristics of population inversion of the $^4I_{13/2}$ level of erbium ions in ytterbium-erbium glasses," *Sov. J. Quantum Electron.*, vol. 11, pp. 1266–1268, 1981.

[15] J. A. Lázaro, M. A. Rebolledo, and J. A. Vallés, "Modeling, characterization and experimental/numerical comparison of signal and fluorescence amplification in Ti:Er:$LiNbO_3$ waveguides," *IEEE J. Quantum Electron.*, vol. 37, no. 11, pp. 1460–1468, Nov. 2001.

[16] E. Tanguy, C. Larat, and J. P. Pocholle, "Modeling of the erbium-ytterbium laser," *Opt. Commun.*, vol. 153, pp. 172–183, 1998.

[17] B. Majaron, M. Čopič, M. Lukač, and M. Marinček, "Influence of hole burning on laser pumping dynamics and efficiency in Yb:Er phosphate glasses," *Proc. SPIE* , vol. 2138, pp. 183–190, 1994.

[18] D. E. McCumber, "Theory of phononterminated optical masers," *Phys. Rev.*, vol. 134, pp. A299–306, 1964.

[19] W. J. Minscalco and R. S. Quimby, "General procedure for the analysis of Er^{3+} cross-sections," *Opt. Lett.*, vol. 16, pp. 258–260, 1991.

[20] E. J. Murphy, Ed., *Integrated Optical Circuits and Components. Design and Applications*. New York: Marcel Dekker, 1999.

[21] R. S. Quimby, "Range of validity of McCumber theory in relating absorption and emission cross-sections," *J. Appl. Phys.*, vol. 92, pp. 180–187, 2002.

Juan A. Vallés was born in Burgos, Spain, on June 12, 1963. He received the B.A., M.Sc., and Ph.D. degrees in physics from the University of Zaragoza, Spain, in 1986, 1987 and 1992, respectively. His doctoral research was centered on a new method for the detection of the hyperfine transitions that are utilized for frequency standards in atomic clocks.

Presently, he is Associate Professor of Optics at the Applied Physics Department, University of Zaragoza, and his current research interests are within the field of erbium-doped waveguide amplifiers and lasers characterization and modeling.

Dr. Vallés is a member of the European Optical Society (EOS) and the Spanish Optical Society (SEDO).

Miguel A. Rebolledo was born in Calatayud, Spain, on October 9, 1947. He received the M.Sc. and Ph.D. degrees in physics from the University of Zaragoza, Zaragoza, Spain, in 1970 and 1973, respectively.

From 1970 to 1975, he was involved in research on atomic spectroscopy. In 1975, he joined the University of Santander, Spain, as Professor of Optics. He was involved in research in photon statistics. In 1984, he moved to the University of Zaragoza, where he has been involved in research on optical fiber and waveguide amplifiers and lasers.

Prof. Rebolledo is a member of the European Optical Society (EOS) and the Spanish Optical Society (SEDO).

Jesús Cortés was born in Cáceres, Spain, on February 4, 1982. He received the B.Sc. degree in physics from the University of Zaragoza, Zaragoza, Spain, in 2004, where he is currently working toward the M.Sc. degree in physics, centered on optics.

Since 2004, he has collaborated with the Applied Physics Department in the group of fiber and waveguide amplifiers and lasers.